# ARTICLES

## Nanostructure Characterization of Carbon Materials with Superwide Pressure Range Adsorption Technique with the Aid of Grand Canonical Monte Carlo Simulation

**M. Sunaga,[†] T. Ohba,[†] T. Suzuki,[§] H. Kanoh,[†,‡] S. Hagiwara,[||] and K. Kaneko*[,†,‡]**

*Department of Chemistry, Faulty of Science, Chiba University, 1-33 Yayoi, Inage, Chiba 263-8522, Japan, Center for Frontier Electronics and Photonics, Chiba University, 1-33, Yayoi, Inage, Chiba 263-8522, Japan, and Department of Environmental Science and Technology, Faculty of Engineering, Shinshu University, 4-17-1 Wakasato, Nagano, 380-8553, Japan, 3-2-16 Kita-machi, Nishitokyo, Tokyo 202-003, Japan*

*Received: August 6, 2003; In Final Form: January 15, 2004*

A new technique of superwide pressure range adsorption (SWPA) isotherm measurement of $N_2$ from $P/P_0 = 10^{-9}$ to 1 at 77 K was developed. The superwide pressure range adsorption isotherms of $N_2$ on activated carbon fiber, molecular sieve carbon, and carbon black were compared with those of their ordinary pressure range isotherms and the simulated isotherms calculated with grand canonical Monte Carlo technique. The SWPA measurement can show the adsorption uptake below $P/P_0 = 10^{-6}$, which is assigned to the adsorption in ultramicropores of pore width < 0.7 nm. The SWPA method shows the presence of ultramicropores even for nonporous carbon black, which has been believed to be nonporous from the ordinary adsorption measurement. Thus, the SWPA method can elucidate the ultramicropore structures of less-crystalline materials.

### 1. Introduction

Molecular probe analysis with vapor adsorption, of which a representative method is $N_2$ adsorption at 77 K, has contributed to the characterization of important less-crystalline porous materials such as nanoporous carbon.[1,2] Recently hydrogen and methane storage subjects have invoked a great interest in nanostructures of carbonaceous materials.[3−9] Also, the high performance of the Li battery and supercapacitor has suggested the elucidation of the nanostructures of carbon materials.[10,11] The representative nanostructures of carbonaceous materials are micropore structures, in particular, ultramicropore structures. IUPAC has classified pores into micropores, mesopores, and macropores using pore width *w*.[12] Here, micropores are pores with $w < 2$ nm. Ultramicropores have small micropores of $w < 0.7$ nm. Micropores have a strong molecule−pore wall interaction potential, inducing micropore filling phenomena; a predominant adsorption begins from an extremely low pressure such as $P/P_0 = 10^{-5}$. It is quite difficult to study micropore filling of vapors in ultramicropores because adsorption is saturated even at a very low pressure region. Accordingly, adsorption measurement from $P/P_0 = 10^{-5}$ is requested for determination of micropore filling. Authors developed the measuring system of the high resolution adsorption isotherm from $P/P_0 = 10^{-5}$ more than 10 years ago;[13] recent commercial equipment enables measurement of the adsorption isotherms from $P/P_0 = 10^{-6}$. However, these measurements cannot provide sufficient information on adsorption in ultramicropores. Also, active studies on pore structures with molecular simulation and density functional theory have been carried out. These studies predict that a predominant $N_2$ adsorption begins below $P/P_0 = 10^{-6}$ for ultramicropores.[14−20] There is no reliable $N_2$ adsorption isotherm covering such a low $P/P_0$ region, and thereby we cannot compare these simulation studies with the experimental one. It is necessary to develop a new technique to measure the $N_2$ adsorption isotherm at 77 K below $P/P_0 = 10^{-6}$. This paper describes that the ultrahigh vacuum (UHV) technique combined adsorption system clearly shows the presence of ultramicroporosity in carbon materials which cannot be evaluated by the usual adsorption method.

### 2. Experimental Section

**2.1. UHV Combined Adsorption System.** The measurement system of the superwide pressure range adsorption (SWPA) consists mainly of the UHV system, high vacuum system, pressure gauges (an ion gauge and 0.1, 10, and 1000 Torr Baratrons), and a laser detector assisted quartz balance system. The whole vacuum system is made of stainless steel. The background pressure is less than $10^{-7}$ Pa. The adsorption measurement below $10^{-5}$ Pa was carried out by the flow method, and adsorption above $10^{-1}$ Pa was measured by the static method. The mean free path of molecules below $10^{-4}$ Pa is greater than 1 m. As the total available length of this SWPA measuring system is less than 1 m, even the flow method can provide adsorption under the quasi-equilibrium conditions. The temperature difference of sample from liquid $N_2$ temperature was measured.[19] The temperature of the sample position was higher than 77 K by 3−5 K below $P/P_0 = 10^{-8}$. The adsorption in ultramicropores of strong interaction potential between a molecule and the ultramicropore was not sensitive to the measuring temperature within 5 K according to preliminary

* Corresponding author. Fax: 81-43-290-2788. E-mail: kaneko@pchem2.s.chiba-u.ac.jp.
[†] Department of Chemistry, Chiba University.
[‡] Center for Frontier Electronics and Photonics, Chiba University.
[§] Shinshu University.
[||] Tokyo Ricoh Co.

10.1021/jp036315t CCC: $27.50 
Published on Web 06/30/2004

examination with the grand canonical Monte Carlo (GCMC) simulation. The sensitivity of the laser detector assisted gravimetry is 0.18 mg. The buoyancy and thermal transpiration effects were corrected.[21,22]

**2.2. Adsorption Measurement.** The SWPA isotherm was measured at liquid $N_2$ temperature after preevacuation of samples at $<10^{-7}$ Pa and 393 K for 2 h. The wide pressure range (WPA) isotherm of $N_2$ from $P/P_0 = 10^{-6}$ range was measured at liquid $N_2$ temperature using the gravimetric equipment after pretreatment at $10^{-3}$ Pa and 393 K for 2 h. Two kinds of nonporous carbon black (no. 32B and no. 4040B, Mitsubishi Chem.) were used. As two carbon black samples have different crystallinities, no. 32B and no. 4040B are called less-crystalline carbon black (l-CB) and well-crystalline carbon black (w-CB) in this article. Two kinds of pitch-based activated carbon fiber (ACF), A5 and A20 (Ad'all), were used. The subtracting pore effect (SPE) method[23,24] using the high resolution $N_2$ adsorption isotherm by the WPA measurement provides that the average pore widths of A5 and A20 are 0.7 and 1.1 nm, respectively. MSC-3A and MSC-5A of molecular sieve carbon (Takeda) were also used. The crystallinity of carbon black samples was examined with X-ray diffraction measurement at 303 K by the transmission method using an angle-dispersive diffractometer (MXP3 system, MAC Science) in the scattering parameter $s$ ($=4\pi \sin\theta/\lambda$) range of 4.2−124 $nm^{-1}$. The monochromatic Mo Kα ($\lambda = 7.093 \times 10^{-2}$ nm) at 50 kV and 30 mA was used for the diffraction measurement. The carbon black samples were observed with a field emission electron scanning microscope (JEOL JSM-6330F).

**2.3. GCMC Simulation.** The $N_2$ adsorption isotherms at 77 K were calculated with GCMC simulation for a graphite slit pore in the $w$ range of 0.4−1.0 nm with every 0.10 nm difference using a one-center approximation. The 12−6 Lennard-Jones potential of $\epsilon_{ff}/k_B = 104.2$ K and $\sigma_{ff} = 0.3632$ nm was used for the $N_2$–$N_2$ interaction. Here $\epsilon_{ff}$ and $\sigma_{ff}$ are the $N_2$ potential well depth and the effective diameter of the $N_2$ molecule. The structureless model using Steele's 10−4−3 potential function was used for the interaction potential of an $N_2$ molecule with a single graphite slab.[25] The fitted parameters of $\epsilon_{sf}$ (0.3632 nm) and $\sigma_{sf}$ ($104.2k_B$ K) of the $N_2$−carbon potential depth and effective diameter, respectively, from the Lorentz−Berthelot rules, were used. Although the parameters used in the 10−4−3 potential function are not shown here, those are shown in the previous works.[14−19] The corrugation nature of the pore wall must be taken into account in simulation of gas adsorption in ultramicropores. We compared the structureless model with the atomistic one for pores from 0.4 to 0.7 nm in width; a considerable discrepancy was observed for the pore of 0.4 nm and the discrepancy was not important for pores of more than 0.5 nm. Although we must be cautious for discussion on adsorption in pores of less than 0.5 nm, only simulation results by the structureless model was used for the present analysis. The relationship between the pore width $H$ of the intercarbon plane distance and the experimental pore width $w$ was approximated by[26]

$$w = H - (2z_0 - \sigma_{ff}), \qquad z_0 = 0.856\sigma_{sf} \tag{1}$$

where $z_0$ is the closest approach between an $N_2$ molecule and the structureless graphite surface.

We used the established GCMC simulation technique.[14,15,27−29] The used rectangular cell size was 6 nm × 6 nm, and this size is replicated two-dimensionally to form an infinite slit-shaped micropore.

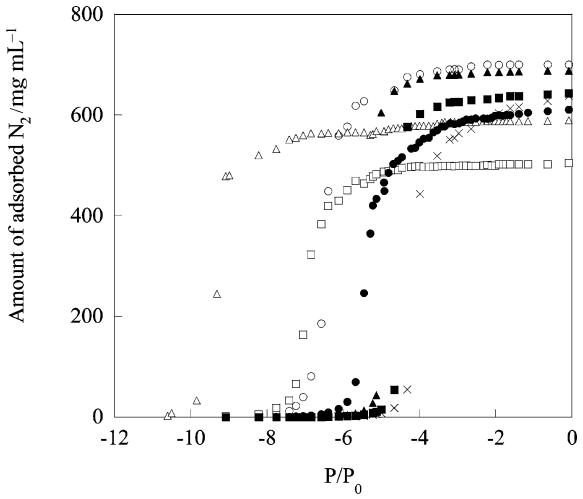


**Figure 1.** Simulated $N_2$ adsorption isotherms of different $w$ values. ○, $w = 0.4$ nm; △, $w = 0.5$ nm; □, $w = 0.6$ nm; ●, $w = 0.7$ nm; ▲, $w = 0.8$; ■, $w = 0.9$; ×, $w = 1.0$ nm.

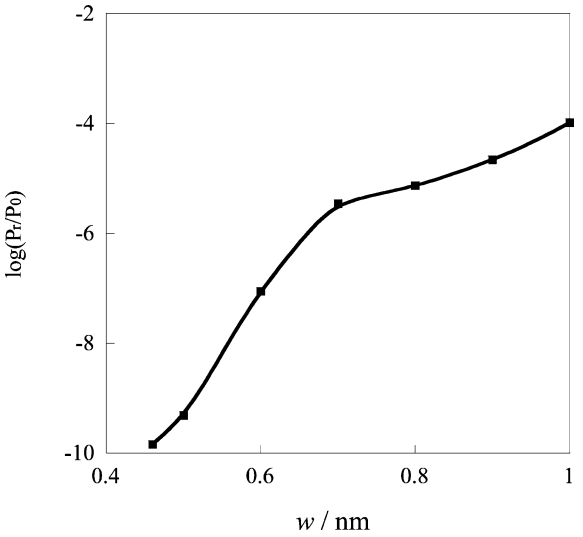


**Figure 2.** The relationship between $Pr/P_0$ and $w$.

## 3. Results and Discussion

**3.1. The Relationship between Rising Relative Pressure and Pore Width.** Figure 1 shows simulated $N_2$ adsorption isotherms of different $w$ values. As GCMC simulation gives rise to no blocking effect for further adsorption even in the case of the ultramicropore, an ideal rising relative pressure $Pr/P_0$ can be obtained under the assumption of the perfect slit pore between the structureless graphite surfaces. Here, $Pr/P_0$ indicates the relative pressure at which the adsorption isotherm rises steeply; the $Pr/P_0$ of the simulated isotherms was determined by extrapolation of the rising line to the abscissa above $w = 0.46$ nm. The repulsive interaction becomes predominant for $w <$ 0.46 nm, inducing an increase of $Pr/P_0$ with the decrease of $w$. We will focus just on the pores in which the attractive interaction is predominant. For $w \geq 0.46$ nm, the log $Pr/P_0$ vs $w$ relation can be approximated by two lines, as shown in Figure 2. Both lines are given by

$$\log(Pr/P_0) = aw + b \tag{2}$$

where $a = 19.29$ $nm^{-1}$ and $b = -18.85$ for $w = 0.46-0.70$ nm and $a = 5.74$ $nm^{-1}$ and $b = -9.76$ for $w = 0.70-1.00$ nm. Consequently, if we determine $P_r/P_0$ experimentally, the $w$ value

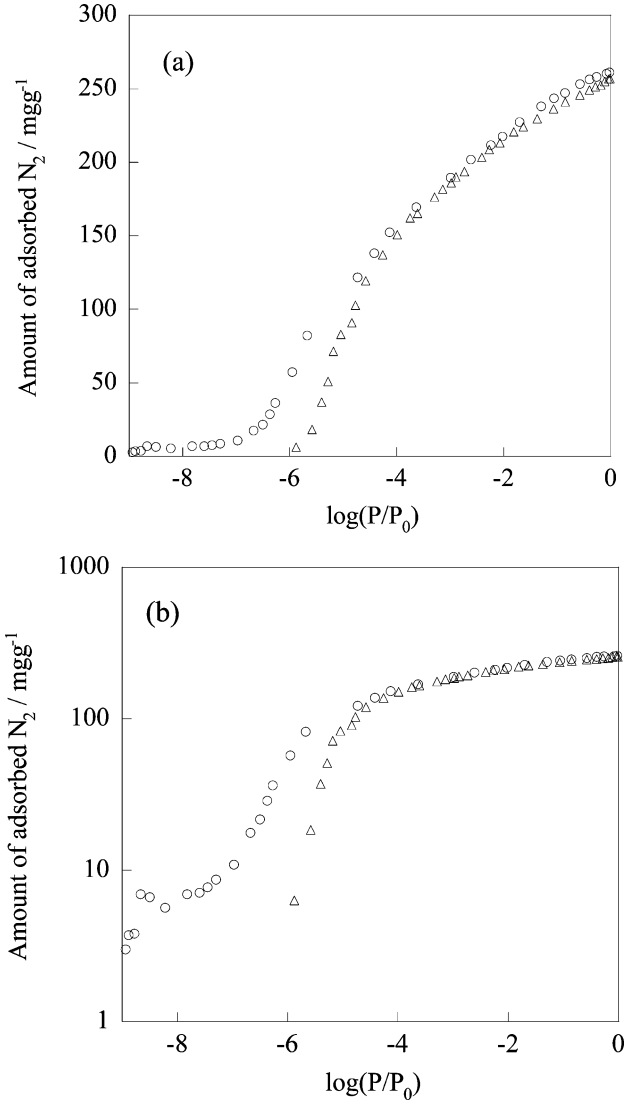


**Figure 3.** $N_2$ adsorption isotherms of A5 at 77 K. ○, SWPA; △, WPA.

can be given using the above relation under the limitation of the perfect slit model.

$N_2$ adsorption isotherms of A5 at the liquid $N_2$ temperature, which were determined by SWPA and WPA measuring systems, are compared with each other in Figure 3. Here the abscissa is expressed by the logarithm of $P/P_0$ for Figure 3a,b; the ordinate of Figure 3b is expressed by the logarithm of the amount of adsorption. The SWPA and WPA isotherms almost overlap each other above $P/P_0 = 10^{-4}$. However, an explicit deviation below $P/P_0 = 10^{-5}$ is observed. Figure 3b shows the presence of the plateau region below $P/P_0 = 10^{-7}$. The adsorption corresponding to the plateau below $P/P_0 = 10^{-7}$ was evaluated by the Langmuir plot. The obtained value is 3.5 mg g$^{-1}$ ($4.3 \times 10^{-3}$ mL g$^{-1}$), which is only 1.3% of total adsorption. As the observed adsorption begins at about $P/P_0 = 10^{-9}$, eq 2 suggests the presence of ultramicropores of $w = 0.5$ nm. Thus, A5 has ultramicropores of $w = 0.5$ nm; the contribution to the total microporosity is not essential for A5 of $w = 0.7$ nm.

Figure 4 shows the logarithmic expression of the $N_2$ adsorption isotherms of A20. An evident discrepancy between two isotherms is observed below $P/P_0 = 10^{-6}$ regardless of almost agreement above $P/P_0 = 10^{-4}$. Accordingly, the sharp increase of the WPA isotherm around $P/P_0 = 10^{-6}$ has no accurate information on the pore structure; the established pore structure analysis using the WPA isotherms underestimates the contribution of ultramicropores. On the contrary, the SWPA method can lead to precise information on ultramicropores. As the SWPA isotherm has a gradual increase with $P/P_0$ even below $P/P_0 = 10^{-6}$, the ultramicropores that cannot be evaluated by the WPA isotherm measurement should have a pore size distribution below $w = 0.6$ nm. The contribution of the small ultramicropores to the total micropore volume is only 0.4%. Therefore, these ultramicropores are not important in the adsorption function of ACF. These results on ACF show the effectiveness of the SWPA technique for elucidation of the ultramicropores. The reason that the SWPA method is powerful for the ultramicropore characterization is as follows. The SWPA system can dose a tiny amount of $N_2$ gas subsequently from $P/P_0 = 10^{-12}$ range, intervening in the pore blocking effect at the entrance of the ultramicropores.

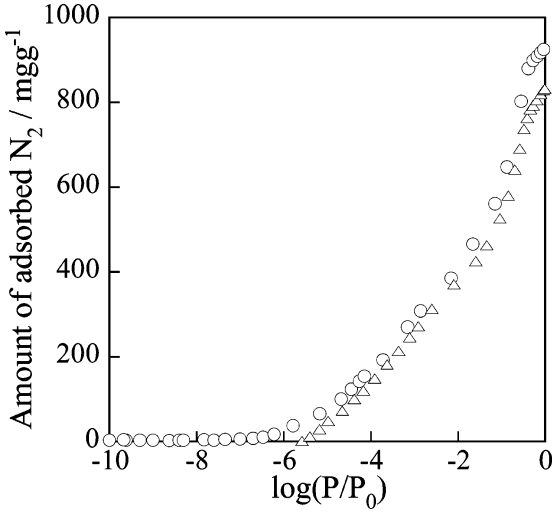


**Figure 4.** $N_2$ adsorption isotherms of A20 at 77 K. ○, SWPA; △, WPA.

**3.2. Ultramicropore Characterization of Molecular Sieve Carbon.** The micropore widths of MSC-3A and MSC-5A are not well-known. The micropore width of molecular sieve carbon is determined using the molecular size dependence of the adsorption rate; it is believed that the pore widths of MSC-3A and MSC-5A are 0.3 and 0.5 nm, respectively. However, the preceding study on MSC-5A showed that water adsorption at 303 K and $N_2$ adsorption at 77 K lead to 0.176 mL g$^{-1}$ and 0.186 mL g$^{-1}$ of the micropore volume, respectively, using the liquid densities of water and $N_2$ at each measuring temperature.[30] The brief coincidence suggests that even $N_2$ adsorption at 77 K can evaluate the average pore width of MSC-5A. In the study authors proposed that the GCMC-simulation-assisted gas adsorption at 303 K provides the entrance pore width of molecular sieve carbons; the evaluated pore widths of MSC-3A and MSC-5A are 0.46 and 0.60 nm, respectively. Therefore, detailed analysis of molecular sieve carbons with this SWPA technique is expected to give an important insight to the ultramicropore structures.

Figure 5 shows the $N_2$ adsorption isotherms of MSC-3A at 77 K. The adsorption amount by the WPA method is almost constant (~10 mg g$^{-1}$) over −5 to 0 of the logarithmic $P/P_0$ range. The observed adsorption amount is briefly comparable to the adsorption amount of A5 around $P/P_0 = 10^{-6}$ of the WPA isotherm. This constant adsorption suggests the presence of the ultramicropores whose width is less than 0.6 nm. On the other hand, the SWPA method gives an explicit step at $P/P_0 = 10^{-8}$ and a gradual increase until $P/P_0 = 10^{-2}$, accompanied by a steep rising above $P/P_0 = 10^{-1}$. Equation 2 indicates the

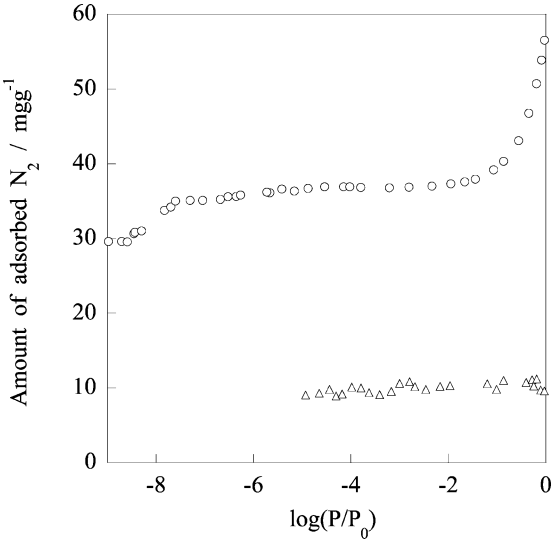


**Figure 5.** $N_2$ adsorption isotherms of MSC-3A at 77 K. ○, SWPA; △, WPA.

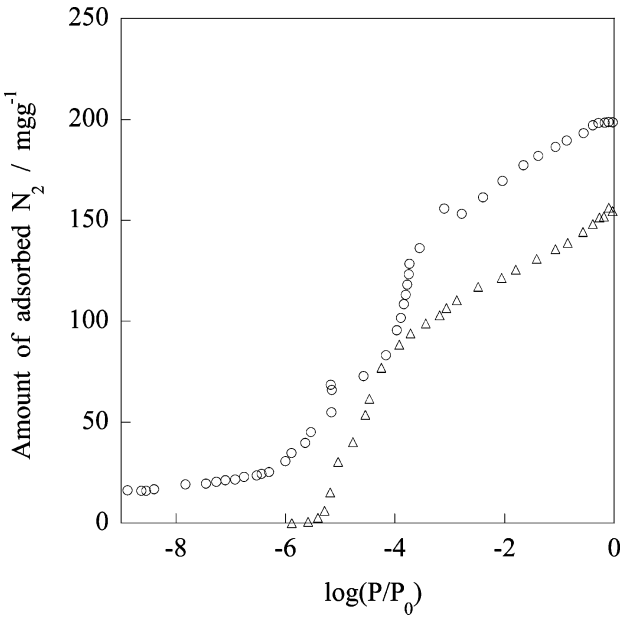


**Figure 6.** $N_2$ adsorption isotherms of MSC-5A at 77 K. ○, SWPA; △, WPA.

presence of the ultramicropores of $w = 0.4$ nm, which should be the pore width of the neck part of the ink bottle type micropores. The steep rising above $P/P_0 = 10^{-1}$ stems from the partial opening of the blocked entrance by the relatively high pressure. The total micropore volume of MSC-3A is estimated to be 0.13 mL g$^{-1}$ from water adsorption at 303 K in the preceding paper.[30] The determined adsorption amount is still 35% of the micropore volume from water adsorption. Therefore, even SWPA technique cannot remove completely the pore blocking effect of the ultramicropores of $w = 0.4$ nm.

Nevertheless, the morphology of the micropores of the ink bottle type and the pore width of the necked ultramicropores can be determined by the SWPA technique. Figure 6 shows the $N_2$ adsorption isotherms of MSC-5A. The WPA isotherm is almost of type I. Then this isotherm was analyzed by the SPE method, leading to the porosity (pore volume = 0.18 mL g$^{-1}$, surface area = 530 m$^2$ g$^{-1}$, and $w = 0.70$ nm). This $w$ value is briefly close to the $Pr/P_0$ deduced from eq 2. Then the $w$ is different from the $w$ value ($w$= 0.5 nm) of MSC-5A determined kinetically. Thus, the kinetic measurement underestimates the ultramicropore width. This is because the kinetic method reflects only the adsorption in the pore entrance and there is no established kinetic theory for evaluation of the pore width, while the static method provides the average pore width of whole pores. The SWPA isotherm shifts upward remarkably, since the WPA method does not evaluate only 28% of the whole pore volume. The SWPA isotherm above $P/P_0 = 10^{-6}$ was analyzed by the SPE method; the accessible pore parameters evaluated by the SWPA method are pore volume = 0.21 mL g$^{-1}$, surface area = 540 m$^2$ g$^{-1}$, and $w = 0.78$ nm. The obtained $w$ value is slightly larger than that evaluated from $P_r/P_0$ with eq 2.

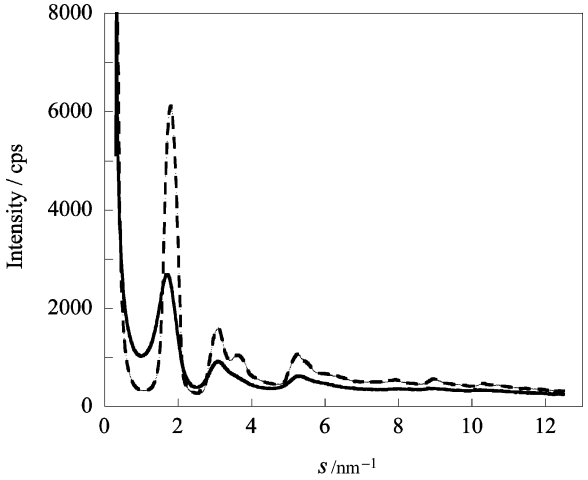


**Figure 7.** X-ray diffraction patterns of CBs. —, w-CB; ---, l-CB.

**TABLE 1: X-ray Scattering Parameters of CBs**

| | $d_{002}$ (nm) | $L_c$ (nm) | $L_a$ (nm) |
|---|---|---|---|
| w-CB | 0.35 | 1.5 | 2.9 |
| l-CB | 0.37 | 1.1 | 2.6 |

Almost constant uptake below $P/P_0 = 10^{-6}$ indicates the presence of ultramicropores of $w < 0.5$ nm. As the contribution of adsorption in those ultramicropores ($w < 0.5$ nm) is 10% of the total pore volume, the average pore width of MSC-5A must be in the range of 0.5−0.75 nm.

Thus, the SWPA method is a powerful technique to evaluate the ultramicropore structures of molecular sieve carbon, which cannot be determined by the conventional WPA method.

**3.3. Ultramicropore Characterization of Nonporous Carbon Black.** X-ray diffraction patterns of nonporous carbon black samples (w-CB and l-CB) are shown in Figure 7. The intensity of w-CB is much higher than that of l-CB. The higher intensity stems from a better crystallinity of w-CB. Both carbon black samples have strong small-angle X-ray scattering (SAXS) below the first peak of the 002 reflection. Therefore, both samples have a heterogeneous electron density structure due to pores, although these carbon black samples do not show open porosity by ordinary $N_2$ adsorption measurement using the WPA method according to the previous study.[13] The interlayer distance $d_{002}$, stack height $L_c$, and stack width $L_a$ of the crystallites are shown in Table 1. Here $L_c$ and $L_a$ were determined by use of the Debye−Scherrer equation. w-CB has the shorter $d_{002}$ and larger crystallite size than l-CB. In particular, the $d_{002}$ of w-CB is 0.35 nm, which is considerably close to the perfect graphite value (0.335 nm). On the other hand, the $d_{002}$ of l-CB is 0.37 nm, indicating a highly disordered structure of nano-order crystallites.

Figure 8 shows field emission SEM images of CB. CB particles are spherical, and their diameters of spheres are similar. The SEM image shows that w-CB consists of primary particles

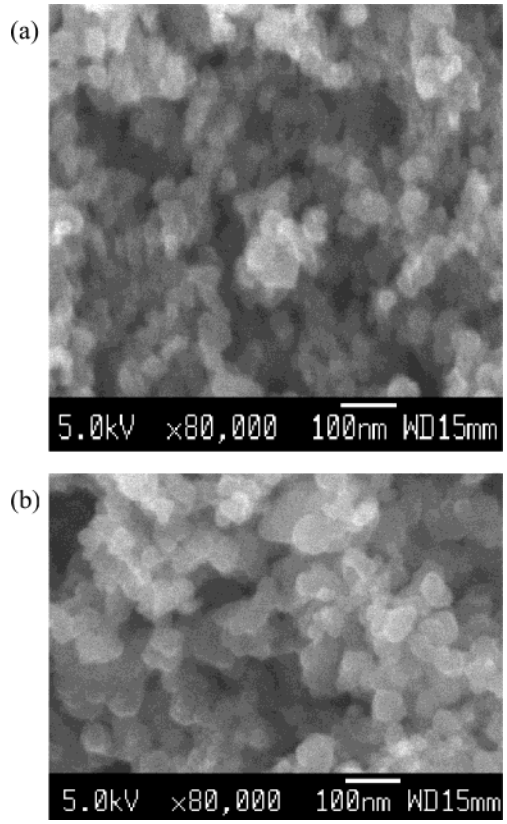


**Figure 8.** Field emission SEM images of CBs. (a) w-CB; (b) l-CB.

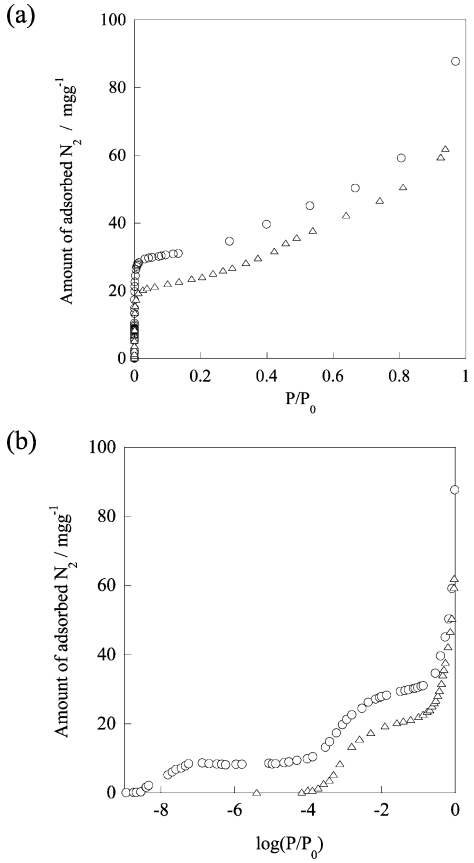


**Figure 9.** $N_2$ adsorption isotherms of w-CB at 77 K. ○, SWPA; △, WPA.

smaller than those of l-CB. As these primary particles form the secondary aggregate, geometric evaluation of the specific surface area is quite difficult. The specific surface area was estimated from a simple geometric calculation using the particle density $\rho_p$ and the spherical diameter $d_p$, assuming the absence of open pores. The $\rho_p$ and $d_p$ for both samples are shown in Table 1. The specific surface areas $a_g$ from the SEM images are 68 $m^2$ $g^{-1}$ for w-CB and 52 $m^2$ $g^{-1}$ for l-CB. If the $a_g$ value agrees with the BET surface area, these carbon blacks are called nonporous ones. Here we used the size of the primary particles in the solid aggregate for w-CB, although primary particles are aggregated with each other to reduce the effective surface area. Consequently, the surface area of w-CB should be overestimated.

Figure 9 shows $N_2$ adsorption isotherms of w-CB. Here Figure 9a shows that both WPA and SWPA isotherms are representatives of type II of IUPAC classification. The shape of the isotherm is indicative of nonporosity. However, the SWPA isotherm shifts upward. The BET plot of the WPA isotherm gives a complete straight line, as shown in Figure 11. The BET surface area from the WPA isotherm is 56 $m^2$ $g^{-1}$, being smaller than the surface area estimated from the SEM observation, should be overestimated. Accordingly, w-CB may be presumed to be a nonporous solid from the conventional WPA analysis, as mentioned above. l-CB has also a type II isotherm, giving good agreement between the BET surface area and that from the SEM observation. Why does the SWPA isotherm shift upward in Figure 9a? The detailed information is shown in Figure 9b. The SWPA isotherm has a clear step at $P/P_0 = 2 \times 10^{-8}$, accompanying a wide plateau region until $P/P_0 = 10^{-4}$. This low pressure uptake must be caused by the presence of open ultramicroporosity, which cannot be evidenced by the WPA method. Equation 2 provides the presence of ultramicropores of $w = 0.55$ nm. As the presence of the step and plateau guarantees ultramicroporosity, we must conclude that additional adsorption in the uniform ultramicropores of $w = 0.55$ nm is observed only by the SWPA method. The pore width of 0.58 nm is very close to that of MSC-3A, which cannot be evaluated by the WPA method because of an intense pore blocking effect. Consequently, w-CB has open ultramicropores which are evidenced by the SWPA method. Thus, the upward shift stems from adsorption in uniform ultramicropores. This conclusion agrees with the strong SAXS shown in Figure 6. The $n_{ad,ul}$, which is the amount adsorbed in ultramicropores, can be evaluated by the Langumir plot, giving $n_{ad,ul} = 8.1$ mg $g^{-1}$, which corresponds to 0.010 mL $g^{-1}$ using the liquid $N_2$ density. Although adsorption in the ultramicropores is about 10% of total adsorption, the absolute potential for an effective adsorption in ultramicropores should be quite low. Also, the pore blocking effect works to the ultramicropores in the case of ordinary $N_2$ adsorption measurement at 77 K. Therefore, w-CB behaves as if it had no open pores. The SWPA isotherm of l-CB has a similar additional adsorption below $P/P_0 = 10^{-4}$, although there is no plateau as observed in w-CB. The additional adsorption below $P/P_0 = 10^{-4}$ gradually increases with $P/P_0$, suggesting that the ultramicropores have less uniformity than those of w-CB. The obtained $n_{ad,ul}$ of l-CB is 8.8 mg $g^{-1}$, similar to that of w-CB. The SWPA isotherms after subtraction of the $n_{ad,ul}$ for w-CB and l-CB are compared with their WPA isotherms in Figure 10. The subtracted SWPA isotherm of w-CB well overlaps the WPA isotherm, supporting the above conclusion that w-CB has uniform ultramicropores which cannot be evaluated by the WPA method, but can be evaluated by the SWPA method.

The excellent coincidence is guaranteed by the comparison of the BET plot for the subtracted SWPA and WPA isotherms of w-CB, as shown in Figure 11. The BET surface areas from the subtracted SWPA and WPA isotherms of w-CB are 53 and

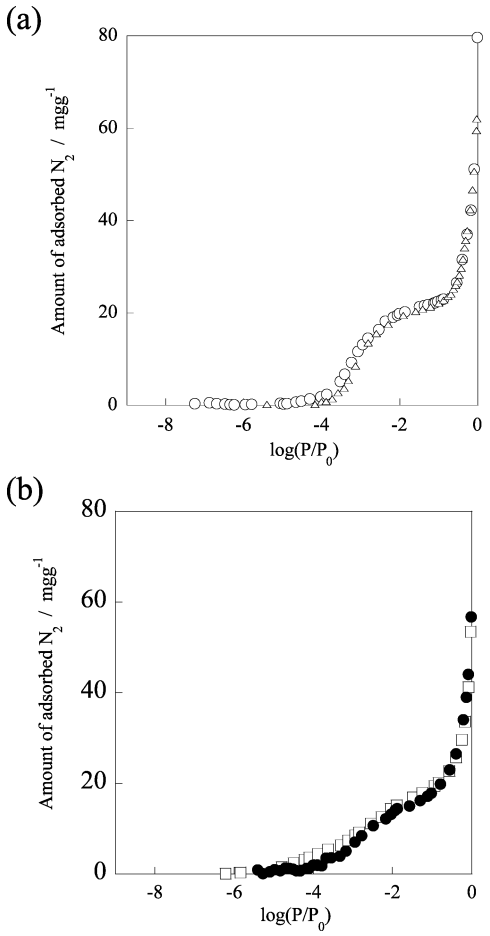


**Figure 10.** $N_2$ adsorption isotherms of CBs at 77 K. ○, subtracted w-CB (SWPA); △, w-CB (WPA); □, subtracted l-CB (SWPA); ●, l-CB (WPA).

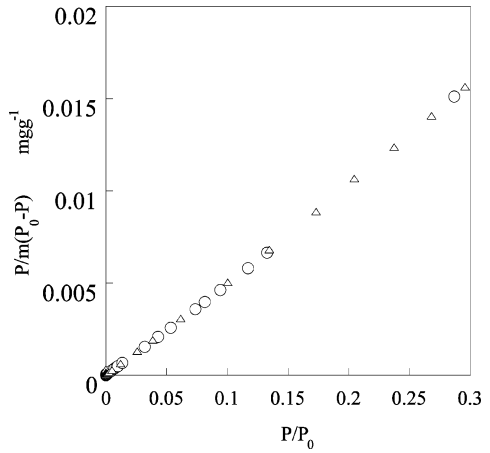


**Figure 11.** BET plots of w-CB. ○, SWPA; △, WPA.

56 $m^2$ $g^{-1}$, respectively. l-CB gave a similar overlapping of the subtracted SWPA and WPA isotherms, but the coincidence is less than that of w-CB. The presence of nonuniform ultramicropores in l-CB results in slight upward deviation of the subtracted SWPA. However, both BET surface areas from the subtracted SWPA and WPA isotherms of l-CB coincide, being 59 $m^2$ $g^{-1}$.

**3.4. Hidden Nanostructured Ultramicropores in Carbon Materials.** The above results and discussion clearly showed that the new SWPA method can elucidate the presence of ultramicroporosity which is not evaluated by the current techniques. As ACF has great micropore volume, the contribution of the ultramicropore elucidated is not predominant in vapor adsorption in micropores. The ultramicropores in ACF should be taken into account in supercritical gases such as He and $N_2$ at an ambient temperature. The entrance structure of ultramicropores of molecular sieve carbon is a key factor in the separation ability. The combined study of the SWPA and WPA methods can show the presence of the necked structure and determine both the pore width of the pore entrance and the average width of the whole range of pores. Recently, authors proposed the GCMC-simulation-assisted gas adsorption method at an ambient temperature to determine the entrance pore widths of MSC-3A and MSC-5A, which are 0.46−0.50 and 0.46−0.50 nm, respectively. These *w* values are close to those estimated from the $P_r/P_0$ value of the SWPA isotherms. The previous TEM examinations of many carbon blacks shows the presence of structural heterogeneities.[31] There are some model structures of carbon black. The representative model is an onion model in which the nanographitic units have a coaxial structure. The ordering of nanographitic units depends on the crystallinity. Therefore, even nonporous carbon black can have open porosity. The intercrystallite structure should not be continuous, offering the ultramicroporosity. However, an $N_2$ molecule of great quadrupole moment can interact specifically with the ultramicropore wall to form an oriented assembly structure fitting the geometric structure of ultramicropore. This kind of stable $N_2$ structure can effectively block the further adsorption of $N_2$ molecules at 77 K. Then we must suppress the assembly structure formation of $N_2$ molecules at the pore entrances during diffusion from the entrance to the deep part of ultramicropores. The SWPA method enables the dosing of a slight number of molecules from an extremely low $P/P_0$ region, leading to the observed additional adsorption in the low $P/P_0$ region. Sweatman and Quirke suggested the presence of micropores of 0.9 nm in width in nonporous carbon black from molecular simulation analysis of $N_2$ adsorption isotherm measured from $P/P_0 = 10^{-6}$, although micropores of their carbon black are larger than those of our carbon black.[32] The evidence for the presence of ultramicropores in nonporous carbon black in this study should show the importance of open structural heterogeneities in carbon black. Also, it is hoped that this new method will elucidate the nanostructures in important novel carbons such as single walled carbon nanotubes, single walled carbon nanohorns, and carbon nanofibers.

**Acknowledgment.** This work was funded by a Grant-in-Aid for Scientific Research (S) from the Japanese Government and in part by the Nanocarbon project from the New Energy and Industrial Technology Development Organization of Japan. T.O. was supported by Research Fellowships of the Japan Society for the Promotion of Science for Young Scientists.

## References and Notes

(1) Unger, K. K.; Kreysa, G.; Baselt, J. P. *Characterization of Porous Solid V*; Elsevier: Amsterdam, 2000.

(2) *Fundamentals of Adsorption 7*; Kaneko, K., Kanoh, H., Hanzawa., Eds. Interrnational Adsorption Society: Chiba, 2002.

(3) Dillon, A. C.; Jones, K. M.; Bekkedahk, T. A.; Jones, K. M.; Parilla, P. A.; Heken, M. J. *Nature* **1997**, *386*, 377.

(4) Reich, R.; Zlegler, W. T.; Rogers, K. A. *Ind. Eng. Chem. Process Des. Dev.* **1980**, *19*, 336.

(5) Bena'rd, P.; Chine, R. *Langmuir* **1997**, *13*, 808.

(6) Menon, V. C.; Komarneni, S. *J. Porous Solids* **1998**, *5*, 43.

(7) Wu, X. B.; Chen, P.; Lin, J.; Tan, K. L. *Int. J. Hydrogen Energy* **2000**, *25*, 261.

(8) Chambers, A.; Park, C.; Baker, R. T. K.; Rodriguez, N. M. *J. Phys. Chem. B* **1998**, *102*, 4253.

(9) Dagani, R. *Chem. Eng. News.* **2002**, *Jan*, 25.

(10) Ago, H.; Nagata, K.; Yoshizawa, K.; Tanaka, K.; Yamabe, T. *Bull. Chem. Soc. Jpn.* **1997**, *70*, 1717.
(11) Tanahasi, I.; Yoshida, A.; Nishino, A. *J. Electrochem. Soc*. **1990**, 137.
(12) Sing, K. S. W.; Everett, D. H.; Haul, R. A. W.; Moscou, L.; Pierotti, R. A.; Rouquerol, J.; Siemieniewska, T. *Pure. Appl. Chem.* **1985**, *57*, 603.
(13) Kakei, K.; Ozeki, S.; Suzuki, T.; Kaneko, K. *J. Chem. Soc., Faraday. Trans.* **1990**, *86*, 371.
(14) Seaton, N. A.; Walton, J. P. R. B.; Quirke, N. *Carbon* **1991**, 27.
(15) Lastoskie, C.; Gubbins, K. Z.; Quirke, N. *J. Phys. Chem*. **1993**, *97*, 4786.
(16) Olivier, J. P. *J. Porous Matter* **1995**, *2*, 9.
(17) Neimark, A. V.; Ravikovitch, P. I. *Langmuir* **1997**, *13*, 5148.
(18) El-Merraoui, M.; Aoshima, M.; Kaneko, K. *Langmuir* **2000**, *16*, 4300.
(19) Ohaba, T.; Murata, K.; Kanho. *Nano Lett*. **2001**, *1*, 371.
(20) Tanaka, H.; El-Merraoui, M.; Steele, W. A.; Kaneko, K. *Chem. Phys. Lett.* **2002**, *352*, 334.
(21) Murata, K.; El-Merraoui, M.; Kaneko, K. *J. Chem. Phys*. **2001**, *114*, 4196.
(22) Takaishi, T.; Sensui, Y. *Trans. Faraday Soc*. **1963**, *53*, 2503.
(23) Setoyama, N.; Suzuki, T.; Kaneko, K. *Carbon* **1998**, *36*, 1459.
(24) Kaneko, K.; Ishii, C.; Kanoh, H.; Hanzawa, Y.; Setoyama, N.; Suzuki, T. *Adv. Colloid Interface Sci*. **1998**, *76*−*77*, 295.
(25) Steele, W. A. *Surf. Sci.* **1973**, 36.
(26) Kaneko, K.; Craknell, R. F.; Nicholson, D. *Langmuir* **1994**, *10*, 4606.
(27) Bojan, M. J.; Cheng, C.; Cole, M. W.; Steele, W. A. *Adsorption* **1996**, *2*, 51.
(28) Cracknell, R. F.; Gubbins, K. E.; Maddox, M.; Nicholson, D. *Acc. Chem. Res*. **1995**, *28*, 281.
(29) Ohaba, T.; Kaneko, K. *Langmuir* **2001**, *17*, 3666.
(30) Suzuki, T.; Kobori, R.; Kaneko, K. *Carbon* **2000**, *38*, 630.
(31) Donnet, J.-B.; Bansal, R. C.; Wang, M.-J. *Carbon Black*; Marcel Dekker: New York, 1993.
(32) Sweatman, M. B.; Quirke, N. *Langmuir* **2001**, *17*, 5011.